

Functionally-graded drug delivery systems with binding reactions: analytical and stochastic approaches for the fraction of drug released

Obi A. Carwood* and Elliot J. Carr

School of Mathematical Sciences, Queensland University of Technology (QUT), Brisbane, Australia

Abstract

Mathematical modelling and computer simulation are increasingly being used alongside experiments to help optimise and guide the design of drug delivery systems. Recent drug delivery research has (i) highlighted the advantages of drug delivery systems constructed using functionally graded materials to achieve target release rates and desired dosage levels over time; and (ii) revealed how it is possible for drug to bind to the carrier material and become irreversibly immobilised within the system, reducing the amount of drug delivered. In this paper, we consider the effect of functionally graded materials and binding reactions on drug release from common slab, cylinder and sphere devices. In particular, two key contributions are presented. First, we outline a deterministic-continuum approach that develops exact analytical expressions for calculating the total fraction of drug released from the device based on a partial differential equation model of the release process. Second, we develop a stochastic-discrete approach for calculating the fraction of drug released over time based on a random-walk model that captures the randomness of the release process and resulting variability in the total fraction of drug released. Both approaches are numerically validated and provide tools for exploring how the fraction of drug released depends on system parameters (e.g. diffusivity and reaction rate functions induced by the functionally graded material and binding reactions), insight which may be useful for designers of drug delivery systems.

1 Introduction

Modelling and simulation are increasingly becoming powerful tools in drug delivery research. Mathematical models improve the fundamental understanding of drug transport and release, provide insights into the effect of device design parameters on drug release profiles, reduce the need for costly and time-consuming experiments, and help optimise and guide the design of drug delivery systems to achieve desired drug release profiles [1–4].

Mathematical models of drug delivery can usually be described as either *deterministic-continuum* or *stochastic-discrete*. Deterministic-continuum models assume the distribution of drug within the device is described by the drug concentration, a continuous function of space changing over time, with a deterministic partial differential equation and appropriate boundary conditions governing drug movement and release, respectively [5–9]. In contrast, stochastic-discrete models assume the distribution of drug within the device is described by the individual positions of drug particles, discrete points in space changing over time, with probabilities governing drug movement and release events [10–14]. Deterministic-continuum models do not account for randomness, may be amenable to analytical solution, and rely on the assumption of a large number of drug particles. On the other hand, stochastic-discrete models account for variability and randomness in the drug release process, hold for small and large numbers of drug particles, and may be computationally prohibitive for a large number of drug particles. Due to these differences, it is important to study both deterministic-continuum and stochastic-discrete models of drug delivery.

Deterministic-continuum models of drug delivery are well established and are typically based on Fick’s second law [2, 6, 8, 11, 15–17], where the spatial and temporal behaviour of the drug concentration is governed by the diffusion equation and specified initial and boundary conditions. Diffusion-only models of this kind yield a drug release profile $F(t)$ (amount of drug released up to time t scaled by the initial amount of drug present in the device) that tends to one in the long time limit (Figure 1). Recent experimental work [18], however, has suggested that some drug particles are never released, likely due to undergoing a

*Corresponding Author (obi.carwood@hdr.qut.edu.au)

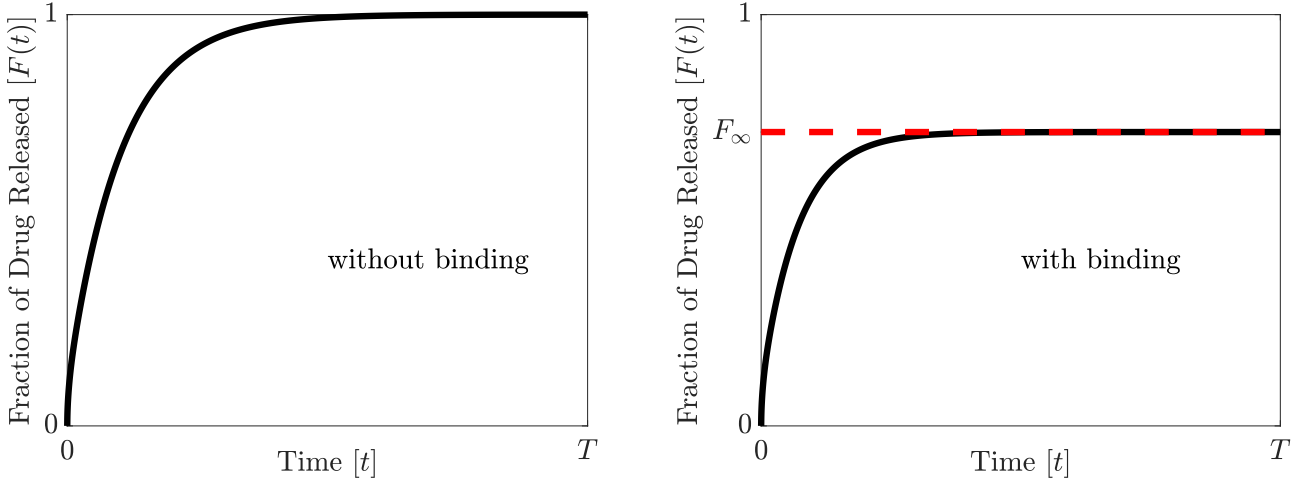


Figure 1: Drug release profiles without/with binding reactions. Typical drug release profiles without binding reactions and with binding reactions, where $F(t)$ is the amount of drug released up to time t scaled by the initial amount of drug present in the device and $F_\infty := \lim_{t \rightarrow \infty} F(t)$ is the fraction of drug released. Note that $F_\infty = 1$ (all drug is released) without binding and $F_\infty < 1$ (some drug is never released) with binding.

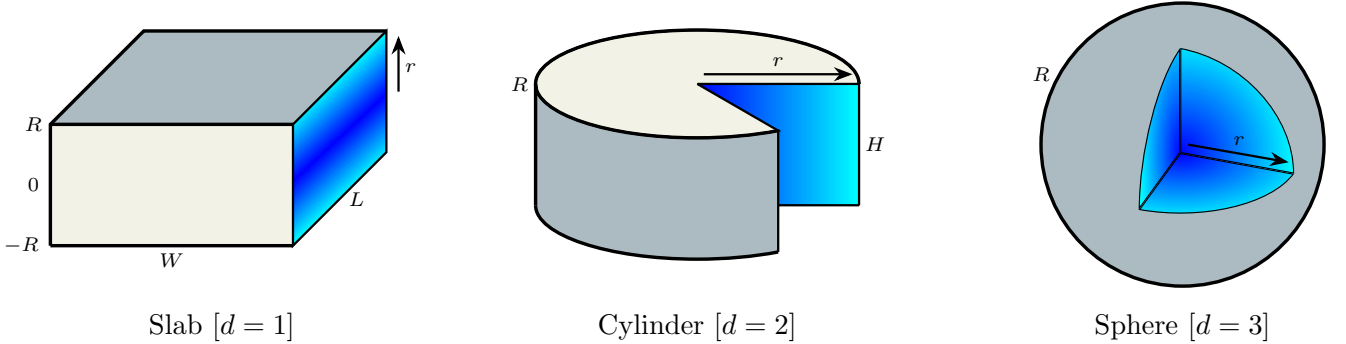


Figure 2: Functionally graded material (FGM) delivery systems. Radially-symmetric FGM delivery devices of slab, cylinder and sphere geometry, all with radius R . The colour gradient highlights the continuously varying material properties (e.g. diffusivity and reaction-rate, see equations (1)–(4)) of the FGM in the direction of the radial coordinate r . For the slab geometry, $L \gg R$ and $W \gg R$, such that the drug release is assumed to be negligible through the minor surfaces of area $2RL$ and $2RW$ relative to the major surfaces of area LW . Similarly, for the cylinder geometry, $H \gg R$, such that the drug release is assumed to be negligible through the minor surfaces of areas πR^2 relative to the major surface of area $2\pi RH$. Slab and cylinder geometries not to scale. Shading (■) indicates the release surfaces and thin coating, which is either fully-permeable or semi-permeable.

chemical reaction and binding to the carrier material [19–21]. This binding mechanism can be captured in deterministic-continuum models by including a first-order reaction term that irreversibly immobilises drug at a specified rate [15, 19, 20, 22]. In this case, resulting reaction-diffusion models yield a drug release profile $F(t)$ that tends (in the long time limit) to a value, F_∞ , which is less than one [15, 22] (Figure 1).

Both deterministic-continuum and stochastic-discrete models of drug delivery are commonly limited to either homogeneous or composite carriers with constant or piecewise-constant material properties (e.g. diffusivity), respectively [5–7, 10, 12–14, 19, 23]. Recently, however, there has been an increase in focus on functionally graded materials (FGMs), which exhibit smooth and continuously varying material properties. The implementation of FGMs have proven to be a promising way to control the drug release, owing to their spatially varying properties, which enable improved control of diffusion kinetics [24–26]. Moreover, the architecture of FGMs allow for drug carrier designs to target specific release rates which offers significant advantages over conventional homogeneous or composite systems [15, 26].

Several recent studies have focussed on binding reactions and/or functional graded materials in the context of deterministic-continuum models of drug delivery. First, [26] proposed a diffusion model for an FGM system of slab geometry without binding reactions, outlining a numerical solution for exploring the drug concentration and drug release profiles. Next, [15] considered a reaction-diffusion model for a spherical FGM system with binding reactions, developing a semi-analytical solution for the drug concentration and drug release profiles. Finally, [22] considered a reaction-diffusion model for homogeneous (monolithic) and

composite (core-shell) systems of slab, cylinder and sphere geometry with binding reactions, developing closed-form expressions for the fraction of drug released (F_∞).

In the current paper, we build on and extend this recent work, presenting two key advances for modelling drug release from functionally-graded delivery systems with binding reactions. First, we outline a deterministic-continuum approach that develops exact analytical expressions for calculating the total fraction of drug released, F_∞ . Second, we develop a stochastic-discrete approach for calculating the fraction of drug released over time, $F(t)$, that captures the randomness inherent in the drug delivery process and the resulting variability in the total fraction of drug released. Underpinning both approaches is the recently established reaction-diffusion model presented in [15], where smooth spatially-varying diffusivity and reaction rate functions accommodate the functionally-graded material and binding reactions. The deterministic-continuum approach shows how F_∞ can be analytically formulated from the governing reaction-diffusion model and exactly resolved via an eigenfunction expansion solution of an appropriate boundary value problem. On the other hand, the stochastic-discrete approach develops a random-walk model of the drug release process by discretising the governing reaction-diffusion model in space and time to derive probabilities governing the movement, binding and release of individual drug particles. Both approaches are valid for radially-symmetric slab, cylinder and sphere devices encapsulated in a thin coating that may be fully-permeable (zero resistance to drug release) or semi-permeable (finite resistance to drug release) (see Figure 2). In summary, the work provides analytical insight into, and computational tools for exploring, the effect of system parameters (diffusivity and reaction rate function induced by the functionally graded material, geometry of the device, coating permeability) on the fraction of drug released, insight which may be useful for designers and manufacturers of drug delivery systems.

The remaining sections of the paper are arranged as follows. Sections 2 and 3 outline our deterministic-continuum and stochastic-discrete approaches, respectively, while section 4 provides numerical experiments validating and demonstrating application of both approaches. Finally, section 5 concludes the work, and provides some possible directions for future research.

2 Deterministic-Continuum Approach

We now outline our deterministic-continuum approach for calculating the total fraction of drug released, F_∞ , for the functionally-graded drug delivery systems considered in this work.

2.1 Reaction-diffusion model

We assume that drug release is governed by the reaction-diffusion model presented in [15]:

$$\frac{\partial c}{\partial t} = \frac{1}{r^{d-1}} \frac{\partial}{\partial r} \left(D(r) r^{d-1} \frac{\partial c}{\partial r} \right) - k(r)c, \quad 0 < r < R, \quad 0 < t < T, \quad (1)$$

$$c(r, 0) = c_0(r), \quad 0 \leq r \leq R, \quad (2)$$

$$\frac{\partial c}{\partial r}(0, t) = 0, \quad (3)$$

$$\begin{cases} c(R, t) = 0, & \text{if fully-permeable,} \\ -D(R) \frac{\partial c}{\partial r}(R, t) = Pc(R, t), & \text{if semi-permeable,} \end{cases} \quad (4)$$

where $d = 1, 2, 3$ for the slab, cylinder, sphere, respectively, R is the radius of the device, $c(r, t)$ is the drug concentration at radius r and time t , T is a specified end time, $c_0(r)$ is the initial concentration profile, P is the mass transfer coefficient characterising the permeability of the thin coating encapsulating the device at $r = R$ (see Figure 2), and $D(r)$ and $k(r)$ are the radially-dependent diffusivity and reaction-rate functions prescribed by the functionally-graded material. The boundary condition at $r = 0$ (3) is the standard boundary condition for radially-symmetric geometries while the boundary condition at $r = R$ (4) describes the standard boundary conditions for fully-permeable or semi-permeable coatings [7].

2.2 Total fraction of drug released

The total fraction of drug released, F_∞ , is defined as the total cumulative amount of drug released from the device scaled by the initial amount of drug present in the device [22]. For the radially-symmetric model

(1)–(4), F_∞ can be expressed as follows

$$F_\infty = \frac{R^{d-1} \int_0^\infty -D(R) \frac{\partial c}{\partial r}(R, t) dt}{\int_0^R r^{d-1} c_0(r) dr}, \quad (5)$$

which is a straightforward generalisation of the formula presented in [22] to accommodate the radially-dependent parameters, $D(r)$, $k(r)$ and $c_0(r)$ (see [Appendix A](#)). One of our primary goals in this paper is to develop analytical expressions that highlight how F_∞ depends on the model parameters: diffusivity, $D(r)$, reaction-rate, $k(r)$, device radius, R , mass transfer coefficient, P , and initial concentration profile, $c_0(r)$. To achieve this, we follow the approach in [22] and introduce the following transformation:

$$C(r) = \int_0^\infty c(r, t) dt, \quad (6)$$

to derive an alternative form for the fraction of drug released. The relevant working, given in [Appendix B](#), shows that F_∞ can be reformulated in terms of $C(r)$:

$$F_\infty = 1 - \frac{\int_0^R r^{d-1} k(r) C(r) dr}{\int_0^R r^{d-1} c_0(r) dr}, \quad (7)$$

and that $C(r)$ satisfies the following boundary value problem:

$$\frac{1}{r^{d-1}} \frac{d}{dr} \left(D(r) r^{d-1} \frac{dC}{dr} \right) - k(r) C = -c_0(r), \quad (8)$$

$$\frac{dC}{dr}(0) = 0, \quad (9)$$

$$\begin{cases} C(R) = 0, & \text{if fully-permeable,} \\ -D(R) \frac{dC}{dr}(R) = PC(R), & \text{if semi-permeable.} \end{cases} \quad (10)$$

Note that this reformulation avoids the full time-dependent solution for $c(r, t)$, which has a significantly more complicated analytical form than $C(r)$.

2.3 Non-dimensionalisation

Before proceeding further, we non-dimensionalise the problem by introducing the following dimensionless variables,

$$\hat{r} := \frac{r}{R}, \quad \hat{C}(\hat{r}) := \frac{C(r)}{C^*}, \quad \hat{D}(\hat{r}) := \frac{D(r)}{D^*}, \quad \hat{k}(\hat{r}) := \frac{R^2}{D^*} k(r), \quad \hat{c}_0(\hat{r}) := \frac{R^2}{C^* D^*} c_0(r), \quad \hat{P} := \frac{PR}{D^*}, \quad (11)$$

where

$$C^* = \max_{r \in [0, R]} c_0(r) \times T, \quad D^* = \max_{r \in [0, R]} D(r).$$

Substituting the dimensionless variables (11) into (7)–(10) yields the following equivalent form for F_∞ (7):

$$F_\infty = 1 - \frac{\int_0^1 \hat{r}^{d-1} \hat{k}(\hat{r}) \hat{C}(\hat{r}) d\hat{r}}{\int_0^1 \hat{r}^{d-1} \hat{c}_0(\hat{r}) d\hat{r}}, \quad (12)$$

where $\hat{C}(\hat{r})$ satisfies the following non-dimensional form of the boundary value problem (8)–(10),

$$\frac{1}{\hat{r}^{d-1}} \frac{d}{d\hat{r}} \left(\hat{D}(\hat{r}) \hat{r}^{d-1} \frac{d\hat{C}}{d\hat{r}} \right) - \hat{k}(\hat{r}) \hat{C} = -\hat{c}_0(\hat{r}), \quad (13)$$

$$\frac{d\hat{C}}{d\hat{r}}(0) = 0, \quad (14)$$

$$\begin{cases} \hat{C}(1) = 0, & \text{if fully-permeable,} \\ -\hat{D}(1) \frac{d\hat{C}}{d\hat{r}}(1) = \hat{P} \hat{C}(1), & \text{if semi-permeable.} \end{cases} \quad (15)$$

While the non-dimensionalised system is only marginally simpler than the original system, the rescaling achieved through non-dimensionalising is important to ensure the magnitude of most model parameters (some of which are often very small [15, 22]) are close to one.

2.4 Analytical solution

To solve the boundary value problem (13)–(15), we adapt previous approaches for dealing with spatially-dependent coefficients [15, 27–29] and expand $\hat{C}(\hat{r})$ in an infinite series involving “simple” eigenvalues and eigenfunctions. Following [15], the eigenvalues $\{\lambda_n, n \in \mathbb{N}^+\}$ and eigenfunctions $\{X_n(\hat{r}), n \in \mathbb{N}^+\}$ are obtained from the following Sturm-Liouville problem:

$$\frac{1}{\hat{r}^{d-1}} \frac{d}{d\hat{r}} \left(\hat{r}^{d-1} \frac{dX_n}{d\hat{r}} \right) = -\lambda_n^2 X_n, \quad (16)$$

$$\frac{dX_n}{d\hat{r}}(0) = 0, \quad (17)$$

$$\begin{cases} X_n(1) = 0, & \text{if fully-permeable,} \\ -\hat{D}(1) \frac{dX_n}{d\hat{r}}(1) = \hat{P} X_n(1), & \text{if semi-permeable,} \end{cases} \quad (18)$$

involving the radially-symmetric Laplace operator and the (already) homogeneous boundary conditions (14)–(15).

Solving the Sturm-Liouville problem (16)–(18), yields the following well-known sets of eigenvalues and eigenfunctions depending on the device geometry ($d = 1, 2, 3$ for the slab, cylinder, sphere, respectively) and the coating permeability (fully-permeable or semi-permeable):

Fully-permeable coating:

$$\lambda_n = \begin{cases} (n - \frac{1}{2}) \pi, & \text{if } d = 1, \\ \text{nth positive root of } J_0(\lambda) = 0, & \text{if } d = 2, \\ n\pi, & \text{if } d = 3, \end{cases} \quad (19)$$

$$X_n(\hat{r}) = \begin{cases} \sqrt{2} \cos(\lambda_n \hat{r}), & \text{if } d = 1, \\ \frac{\sqrt{2}}{J_1(\lambda_n)} J_0(\lambda_n \hat{r}), & \text{if } d = 2, \\ \frac{\sqrt{2} \sin(\lambda_n \hat{r})}{\hat{r}}, & \text{if } d = 3, \end{cases} \quad (20)$$

Semi-permeable coating:

$$\lambda_n = \begin{cases} \text{nth positive root of } \lambda \hat{D}(1) \tan(\lambda) = \hat{P}, & \text{if } d = 1, \\ \text{nth positive root of } \lambda \hat{D}(1) J_1(\lambda) = \hat{P} J_0(\lambda), & \text{if } d = 2, \\ \text{nth positive root of } (\hat{D}(1) - \hat{P}) \tan(\lambda) = \lambda \hat{D}(1), & \text{if } d = 3, \end{cases} \quad (21)$$

$$X_n(\hat{r}) = \begin{cases} \frac{2\sqrt{\lambda_n}}{\sqrt{\sin(2\lambda_n) + 2\lambda_n}} \cos(\lambda_n \hat{r}), & \text{if } d = 1, \\ \frac{\sqrt{2}}{\sqrt{J_0(\lambda_n)^2 + J_1(\lambda_n)^2}} J_0(\lambda_n \hat{r}), & \text{if } d = 2, \\ \frac{2\sqrt{\lambda_n}}{\sqrt{2\lambda_n - \sin(2\lambda_n)}} \frac{\sin(\lambda_n \hat{r})}{\hat{r}}, & \text{if } d = 3, \end{cases} \quad (22)$$

where J_0 and J_1 are, respectively, the order 0 and 1 Bessel functions of the first kind. Note that eigenfunctions are orthogonal and have been normalised to ensure they have length one, that is,

$$\int_0^1 \hat{r}^{d-1} X_n(\hat{r}) X_m(\hat{r}) d\hat{r} = \begin{cases} 1, & \text{if } m = n, \\ 0, & \text{if } m \neq n. \end{cases} \quad (23)$$

With the eigenpairs (λ_n, X_n) identified for all cases, the analytical solution for $\hat{C}(\hat{r})$ is expressed as

$$\hat{C}(\hat{r}) = \sum_{n=1}^{\infty} \alpha_n X_n(\hat{r}), \quad (24)$$

where, due to orthonormality (23), we have

$$\alpha_n = \int_0^1 \hat{r}^{d-1} \hat{C}'(\hat{r}) X_n(\hat{r}) d\hat{r}. \quad (25)$$

To complete the solution procedure, we calculate the coefficients $\{\alpha_n, n \in \mathbb{N}^+\}$ to ensure the solution expansion (24) satisfies the non-dimensionalised ODE (13). This is achieved by substituting (24) into (13)

$$\sum_{n=1}^{\infty} \alpha_n \left(\frac{1}{\hat{r}^{d-1}} \frac{d}{d\hat{r}} \left(\hat{D}(\hat{r}) \hat{r}^{d-1} \frac{dX_n}{d\hat{r}} \right) - \hat{k}(\hat{r}) X_n(\hat{r}) \right) = -\hat{c}_0(\hat{r}),$$

applying the product rule of differentiation

$$\sum_{n=1}^{\infty} \alpha_n \left(\hat{D}'(\hat{r}) X_n'(\hat{r}) + \hat{D}(\hat{r}) \frac{1}{\hat{r}^{d-1}} \frac{d}{d\hat{r}} \left(\hat{r}^{d-1} \frac{dX_n}{d\hat{r}} \right) - \hat{k}(\hat{r}) X_n(\hat{r}) \right) = -\hat{c}_0(\hat{r}),$$

utilising equation (16)

$$\sum_{n=1}^{\infty} \alpha_n \left(\hat{D}'(\hat{r}) X_n'(\hat{r}) - \left(\lambda_n^2 \hat{D}(\hat{r}) + \hat{k}(\hat{r}) \right) X_n(\hat{r}) \right) = -\hat{c}_0(\hat{r}),$$

and, finally, multiplying by $\hat{r}^{d-1} X_m(\hat{r})$ and integrating over $\hat{r} \in [0, 1]$:

$$\sum_{n=1}^{\infty} \alpha_n \int_0^1 \hat{r}^{d-1} \left(\hat{D}'(\hat{r}) X_n'(\hat{r}) X_m(\hat{r}) - \left(\lambda_n^2 \hat{D}(\hat{r}) + \hat{k}(\hat{r}) \right) X_n(\hat{r}) X_m(\hat{r}) \right) d\hat{r} = - \int_0^1 \hat{r}^{d-1} \hat{c}_0(\hat{r}) X_m(\hat{r}) d\hat{r}. \quad (26)$$

Note that equation (26) is linear in the coefficients $\{\alpha_n, n \in \mathbb{N}^+\}$ and hence assembling this equation for each $m \in \mathbb{N}^+$ yields a linear system

$$\mathbf{A} \boldsymbol{\alpha} = \mathbf{b}, \quad (27)$$

where $A_{m,n}$ (entry of \mathbf{A} in row m and column n) and b_m (m th entry of \mathbf{b}) are defined as

$$A_{m,n} = \int_0^1 \hat{r}^{d-1} \left(\hat{D}'(\hat{r}) X_n'(\hat{r}) X_m(\hat{r}) - \left(\lambda_n^2 \hat{D}(\hat{r}) + \hat{k}(\hat{r}) \right) X_n(\hat{r}) X_m(\hat{r}) \right) d\hat{r}, \quad (28)$$

$$b_m = - \int_0^1 \hat{r}^{d-1} \hat{c}_0(\hat{r}) X_m(\hat{r}) d\hat{r}. \quad (29)$$

Solving this linear system for $\boldsymbol{\alpha} = (\alpha_1, \alpha_2, \dots)^T$ provides the coefficients in the solution expansion (24), and thus the analytical solution for $\hat{C}(\hat{r})$ is fully resolved.

2.5 Analytical expressions

Substituting the analytical solution for $\hat{C}(\hat{r})$ (24) into F_{∞} (12) yields an analytical expression for the total fraction of drug released depending on the device geometry (slab, cylinder or sphere) and the coating permeability (fully-permeable or semi-permeable):

Fully-permeable coating:

$$\text{Slab:} \quad F_{\infty} = 1 - \sum_{n=1}^{\infty} \frac{\sqrt{2} \alpha_n}{\int_0^1 \hat{c}_0(\hat{r}) d\hat{r}} \int_0^1 \hat{k}(\hat{r}) \cos(\lambda_n \hat{r}) d\hat{r}, \quad (30)$$

$$\text{Cylinder:} \quad F_{\infty} = 1 - \sum_{n=1}^{\infty} \frac{\sqrt{2} \alpha_n}{|J_1(\lambda_n)| \int_0^1 \hat{r} \hat{c}_0(\hat{r}) d\hat{r}} \int_0^1 \hat{r} \hat{k}(\hat{r}) J_0(\lambda_n \hat{r}) d\hat{r}, \quad (31)$$

$$\text{Sphere:} \quad F_{\infty} = 1 - \sum_{n=1}^{\infty} \frac{\sqrt{2} \alpha_n}{\int_0^1 \hat{r}^2 \hat{c}_0(\hat{r}) d\hat{r}} \int_0^1 \hat{r} \hat{k}(\hat{r}) \sin(\lambda_n \hat{r}) d\hat{r}, \quad (32)$$

Semi-permeable coating:

$$\text{Slab:} \quad F_\infty = 1 - \sum_{n=1}^{\infty} \frac{2\sqrt{\lambda_n}\alpha_n}{\sqrt{\sin(2\lambda_n) + 2\lambda_n} \int_0^1 \hat{c}_0(\hat{r}) d\hat{r}} \int_0^1 \hat{k}(\hat{r}) \cos(\lambda_n \hat{r}) d\hat{r}, \quad (33)$$

$$\text{Cylinder:} \quad F_\infty = 1 - \sum_{n=1}^{\infty} \frac{\sqrt{2}\alpha_n}{\sqrt{J_0(\lambda_n)^2 + J_1(\lambda_n)^2} \int_0^1 \hat{r}\hat{c}_0(\hat{r}) d\hat{r}} \int_0^1 \hat{r}\hat{k}(\hat{r}) J_0(\lambda_n \hat{r}) d\hat{r}, \quad (34)$$

$$\text{Sphere:} \quad F_\infty = 1 - \sum_{n=1}^{\infty} \frac{2\sqrt{\lambda_n}\alpha_n}{\sqrt{2\lambda_n - \sin(2\lambda_n)} \int_0^1 \hat{r}^2 \hat{c}_0(\hat{r}) d\hat{r}} \int_0^1 \hat{r}\hat{k}(\hat{r}) \sin(\lambda_n \hat{r}) d\hat{r}, \quad (35)$$

where the eigenvalues $\{\lambda_n, n \in \mathbb{N}^+\}$ are defined in equations (19) and (21), the coefficients $\{\alpha_n, n \in \mathbb{N}^+\}$ are defined via solution of the linear system (27), and the dimensionless variables are defined in equation (11). Finally, we note that in practice the analytical expressions (30)–(35) are computed using a specified (finite) number of terms, N_s .

3 Stochastic-Discrete Approach

We now outline our stochastic-discrete approach for determining the fraction of drug released based on a random-walk model of the drug delivery process.

3.1 Determination of probabilities

Random walk models of diffusion can be developed by discretising the diffusion model in space and time to derive probabilities governing the movement of individual particles [22, 30–32]. In this paper, we build on this approach and discretise the reaction-diffusion model (1)–(4) in space and time to derive probabilities governing the movement, binding and release of individual drug particles. In this section, we keep the discussion focussed on the semi-permeable coating problem (second boundary condition listed in (4)) and point out important differences when required for the fully-permeable coating problem (first boundary condition listed in (4)). Our random walk model considers N_p individual drug particles with the discretisation of (1)–(4) carried out using uniform spatial and temporal grids, defined by $r_i = (i - 1)h$ for $i = 1, \dots, M$ and $t_n = n\tau$ for $n = 1, \dots, N_t$, where $h = R/(M - 1)$ and $\tau = T/N_t$. To perform the spatial discretisation, we use the standard vertex-centred finite volume method outlined in Appendix C with second-order central differences used to approximate derivative terms and finite volumes spanning the intervals $r \in [w_i, e_i]$ for $i = 1, \dots, M$, where $w_i = \max\{0, (i - 3/2)h\}$ and $e_i = \min\{(i - 1/2)h, R\}$. For the semi-permeable coating problem, this discretisation in space yields a system of ODEs,

$$\frac{d\mathbf{c}}{dt} = \mathbf{A}_m \mathbf{c} - \mathbf{A}_b \mathbf{c} - \mathbf{A}_r \mathbf{c}, \quad \mathbf{c}(0) = \mathbf{c}_0, \quad (36)$$

where $\mathbf{c} = (c_1, \dots, c_M)^\top$ such that $c_i \approx c(r_i, t)$, $\mathbf{c}_0 = (c_0(r_1), \dots, c_0(r_M))^\top$, and \mathbf{A}_m , \mathbf{A}_b , and \mathbf{A}_r denote, respectively, the $M \times M$ discretisation matrices governing movement (diffusion term in equation (1)), binding (reaction term in equation (1)) and release (boundary condition (4)). As evident in Appendix C, \mathbf{A}_m and \mathbf{A}_b are tridiagonal and diagonal matrices, respectively, while \mathbf{A}_r contains a single non-zero entry in row M and column M .

To study the behaviour of individual drug particles, we reformulate the problem using the relationship $c_i = N_i/(S_p V_i)$, where N_i is the number of drug particles within control volume i at time t (assumed located at lattice site i), $V_i = (e_i^d - w_i^d)/d$ and $S_p = \sum_{i=1}^M c_0(r_i) V_i / N_p$ is a scaling constant depending on the initial concentration profile $c_0(r)$ (2). Applying both this relationship and a forward Euler time discretisation to equation (36) yields the following scheme relating the spatial distributions of drug particles at times $t = t_{n+1}$ and $t = t_n$:

$$\mathbf{N}_{n+1}^\top = \mathbf{N}_n^\top \mathbf{P}_m - \mathbf{N}_n^\top \mathbf{P}_b - \mathbf{N}_n^\top \mathbf{P}_r, \quad (37)$$

where $\mathbf{N} = (N_1, \dots, N_M)^\top$, \mathbf{N}_k denotes \mathbf{N} at time $t = k\tau$, $\mathbf{N}_0 = \text{round}(S_p(c_0(r_1)V_1, \dots, c_0(r_M)V_M)^\top)$, $\mathbf{P}_m = \mathbf{V}^{-1}(\mathbf{I} + \tau \mathbf{A}_m^\top) \mathbf{V}$, $\mathbf{P}_b = \tau \mathbf{A}_b^\top$, $\mathbf{P}_r = \tau \mathbf{A}_r^\top$ and $\mathbf{V} = \text{diag}(V_1, \dots, V_M)$. As we discuss below, the entries of \mathbf{P}_m , \mathbf{P}_b and \mathbf{P}_r can be interpreted, respectively, as probabilities governing movement, binding and release events [33] provided the time step τ is constrained appropriately.

Movement probabilities: \mathbf{P}_m is a tridiagonal matrix with non-zero entries:

$$\begin{aligned} p_{1,1}^m &= 1 - \frac{\tau D(e_1)e_1^{d-1}}{V_1 h}, & p_{1,2}^m &= \frac{\tau D(e_1)e_1^{d-1}}{V_1 h}, \\ p_{i,i-1}^m &= \frac{\tau D(w_i)w_i^{d-1}}{V_i h}, & p_{i,i}^m &= 1 - \frac{\tau [D(w_i)w_i^{d-1} + D(e_i)e_i^{d-1}]}{V_i h}, & p_{i,i+1}^m &= \frac{\tau D(e_i)e_i^{d-1}}{V_i h}, \quad \text{for } i = 2, \dots, M-1, \\ p_{M,M-1}^m &= \frac{\tau D(w_M)w_M^{d-1}}{V_M h}, & p_{M,M}^m &= 1 - \frac{\tau D(w_M)w_M^{d-1}}{V_M h}, \end{aligned}$$

where we interpret $p_{i,j}^m$ (entry in row i and column j) as the probability that a drug particle located at lattice site i at time $t = t_n$ moves to lattice site j (remains at lattice site j if $i = j$) at time $t = t_{n+1} = t_n + \tau$ (given that it did not undergo a binding or release event at time $t = t_n$). Studying the above expressions, we note that each row of \mathbf{P}_m sums to 1, which is an expected result as drug particles must undergo a movement event if they did not undergo a binding or release event. For the fully-permeable coating problem, we note further that the movement probabilities apply only at lattice sites $i = 1, \dots, M-1$, since all drug particles located at lattice site N at time $t = t_n$ are immediately released from the device with probability one.

Binding probabilities: \mathbf{P}_b is a diagonal matrix with non-zero entries:

$$p_{i,i}^b = \tau k(r_i), \quad \text{for } i = 1, \dots, M,$$

where we interpret $p_{i,i}^b$ (entry in row i and column i) as the probability that a drug particle located at lattice site i at time $t = t_n$ binds to the carrier material and remains at lattice site i thereafter (given that it did not undergo a release event at time $t = t_n$). For the fully-permeable coating problem, we note that the binding probabilities apply only at lattice sites $i = 1, \dots, M-1$, since all drug particles located at lattice site M at time $t = t_n$ are immediately released from the device with probability one.

Release probabilities: \mathbf{P}_r is a matrix with a single non-zero entry:

$$p_{M,M}^r = \frac{\tau P R^{d-1}}{V_M},$$

where we interpret $p_{M,M}^r$ (entry in row M and column M) as the probability that a drug particle located at lattice site M at time $t = t_n$ is released from the device (and no longer undergoes any movement or binding events). Note that $p_{M,M}^r$ increases for increasing values of P , which agrees intuitively with larger values of the mass transfer coefficient increasing the rate at which drug is released from the device. For the fully-permeable coating problem, we simply take $p_{M,M}^r = 1$, since all drug particles located at lattice site M at time $t = t_n$ are immediately released from the device with probability one.

3.2 Time step constraints

For a valid random walk model we must ensure that all entries of \mathbf{P}_m , \mathbf{P}_b , and \mathbf{P}_r are in $[0, 1]$. Studying the probabilities given in the previous section, this yields a set of conditions on the time step, τ , depending on the coating permeability that must be satisfied simultaneously:

Fully-permeable coating:

$$\begin{aligned} \tau &\leq \min \left\{ \frac{V_1 h}{D(e_1)e_1^{d-1}}, \min \left\{ \frac{V_i h}{D(w_i)w_i^{d-1} + D(e_i)e_i^{d-1}}, i = 2, \dots, M-1 \right\} \right\}, \\ \tau &\leq \min \left\{ \frac{1}{k(r_i)}, i = 1, \dots, M-1 \right\}, \end{aligned}$$

Semi-permeable coating:

$$\begin{aligned} \tau &\leq \min \left\{ \frac{V_1 h}{D(e_1)e_1^{d-1}}, \min \left\{ \frac{V_i h}{D(w_i)w_i^{d-1} + D(e_i)e_i^{d-1}}, i = 2, \dots, M-1 \right\}, \frac{V_M h}{D(w_M)w_M^{d-1}} \right\}, \\ \tau &\leq \min \left\{ \frac{1}{k(r_i)}, i = 1, \dots, M \right\}, \\ \tau &\leq \frac{V_M}{P R^{d-1}}. \end{aligned}$$

Note that the conditions for the fully-permeable coating are less restrictive than those for the semi-permeable coating due to the absence of any conditions arising from lattice node M , where drug particles are immediately released from the device.

3.3 Random walk algorithm

Using the stochastic-discrete approach, the fraction of drug released over time can be calculated by simply tracking the cumulative number of drug particles released over time. Formally, we have

$$F(t_n) = \frac{N_r(t_n)}{N_p}, \quad \text{for } n = 1, \dots, N_t,$$

where $N_r(t_n)$ is the number of drug particles released between $t = 0$ and $t = t_n$ and N_p is the total number of drug particles initially loaded into the device. The total fraction of drug released is then given by $F_\infty = F(t_{N_t}) = F(T)$, where we assume T (or equivalently N_t) is large enough to ensure there are no longer any active drug particles remaining in the device (all particles have undergone either a binding event or a release event). Algorithm 1 summarises the movement, binding and release of individual drug particles and the stochastic-discrete approach for calculating the fraction of drug released.

Algorithm 1 (Random Walk Model)

```

 $C_{i,0} = c_0(r_i)$  for all  $i = 1, \dots, M$  % initial concentration at lattice site  $i$ 
 $S = \sum_{i=1}^M C_{i,0} V_i / N_p$  % scaling constant
 $N_{i,0} = \text{round}(C_{i,0} V_i / S)$  for all  $i = 1, \dots, M$  % initial number of particles at lattice site  $i$ 
 $N_p = \sum_{i=1}^M N_{i,0}$  % adjusted total number of particles
 $k = 0$  % initialise particle index
for  $i = 1, \dots, M$  % loop over lattice sites
     $X_{p,0} = i$  for all  $p = k + 1, \dots, k + N_{i,0}$  % initial lattice site of particle  $p$ 
     $k = k + N_{i,0}$  % update particle index
end
 $N_r(t_0) = 0$  % initial number of released particles at  $t = t_0 = 0$ 
 $A_p = \text{true}$  for all  $p = 1, \dots, N_p$  % set active status as initially true for all particles
 $P_{i,0} = 0$  and  $P_{i,j} = \sum_{z=1}^j p_{i,z}^m$  for all  $i = 1, \dots, M$  and  $j = 1, \dots, M$  % cumulative movement probabilities
for  $n = 1, \dots, N_t$  % loop over time steps
     $N_r(t_n) = N_r(t_{n-1})$  % number of particles released at  $t = t_{n-1}$ 
    for  $p = 1, \dots, N_p$  % loop over number of particles
        if  $A_p$  true and  $X_{p,n-1} = M$  % check if particle is currently active and at end lattice site
            if fully-permeable coating
                 $N_r(t_n) = N_r(t_n) + 1$  and  $A_p = \text{false}$  % release particle
            else if semi-permeable coating
                Sample  $q \sim \text{Uniform}(0, 1)$  % uniform random number in  $[0, 1]$ 
                If  $q \in (0, p_{M,M}^r)$  then  $N_r(t_n) = N_r(t_n) + 1$  and  $A_p = \text{false}$  % release particle
            end
        end
        if  $A_p$  true % check if particle is still currently active
            Sample  $q \sim \text{Uniform}(0, 1)$  % uniform random number in  $[0, 1]$ 
            If  $q \in (0, p_{i,i}^b)$  then  $A_p = \text{false}$  % bind particle
        end
        if  $A_p$  true % check if particle is still currently active
            Sample  $q \sim \text{Uniform}(0, 1)$  % uniform random number in  $[0, 1]$ 
            Find  $j$  such that  $q \in (P_{i,j-1}, P_{i,j})$ , then  $X_{p,n} = j$  % move particle
        end
    end
     $F(t_n) = N_r(t_n) / N_p$  % fraction of drug released at  $t = t_n$ 
end
 $F_\infty = F(t_n)$  % total fraction of drug released

```

4 Results

4.1 Diffusivity and reaction-rate functions

Applying the deterministic-continuum (section 2) and stochastic-discrete (section 3) approaches requires choosing appropriate diffusivity and reaction-rate functions, $D(r)$ and $k(r)$, to characterise the heterogeneity of the FGM. In this work, we use standard smooth approximations to the step-wise functions

$$D(r) = \begin{cases} D_{\max}, & 0 < r < \sigma, \\ D_{\min}, & \sigma < r < R, \end{cases} \quad (38)$$

$$k(r) = \begin{cases} k_{\min}, & 0 < r < \sigma, \\ k_{\max}, & \sigma < r < R, \end{cases} \quad (39)$$

where $D_{\max} > D_{\min}$ and $k_{\max} > k_{\min}$. Following previous work [15], we choose

$$D(r) = D_{\max} + (D_{\min} - D_{\max}) \left(\frac{1}{2} + \frac{1}{\pi} \arctan \left(\frac{\alpha(r - \sigma)}{R} \right) \right), \quad (40)$$

$$k(r) = k_{\min} + (k_{\max} - k_{\min}) \left(\frac{1}{2} + \frac{1}{\pi} \arctan \left(\frac{\alpha(r - \sigma)}{R} \right) \right), \quad (41)$$

where α and σ are parameters controlling the steepness and location of the transition between the stepwise values, respectively. Note that $D(r)$ and $k(r)$ are decreasing and increasing functions of r , respectively, and can be considered as corresponding to an FGM exhibiting a decreasing porosity as r increases [15].

For a specified value of α , we follow [15] and determine a corresponding value of σ to ensure the average diffusivity across the slab ($d = 1$), cylinder ($d = 2$) and sphere ($d = 3$) geometries remains fixed. In particular, for each d , we enforce that

$$\frac{d}{R^d} \int_0^R r^d D(r) dr = D_{\text{avg}}, \quad (42)$$

where D_{avg} is chosen as the average diffusivity of the step-wise function (38) over $[0, R]$ when $\sigma = R/2$:

$$D_{\text{avg}} = \frac{d}{R^d} \left(\int_0^{R/2} r^d D_{\max} dr + \int_{R/2}^R r^d D_{\min} dr \right) = \frac{1}{2^d} D_{\max} + \left(1 - \frac{1}{2^d} \right) D_{\min}. \quad (43)$$

For a specified value of α , we therefore determine a corresponding value of σ by solving the following nonlinear equation (for further details on the numerical procedure employed, the interested reader is referred to our MATLAB code available on GitHub; see [Data availability](#)):

$$\frac{d}{R^d} \int_0^R r^d \left(D_{\max} + (D_{\min} - D_{\max}) \left(\frac{1}{2} + \frac{1}{\pi} \arctan \left(\frac{\alpha(r - \sigma)}{R} \right) \right) \right) dr = D_{\text{avg}}. \quad (44)$$

In the case of $k(r)$, the same values for α and σ are used, which equivalently ensures that the average reaction rate is maintained across the slab ($d = 1$), cylinder ($d = 2$) and sphere ($d = 3$) geometries, that is,

$$\frac{d}{R^d} \int_0^R r^d k(r) dr = k_{\text{avg}}, \quad (45)$$

where k_{avg} is the average reaction-rate of the stepwise function (39) over $[0, R]$ when $\sigma = R/2$:

$$k_{\text{avg}} = \frac{1}{2^d} k_{\min} + \left(1 - \frac{1}{2^d} \right) k_{\max}. \quad (46)$$

For each of the slab ($d = 1$), cylinder ($d = 2$) and sphere ($d = 3$) geometries, Figure 3 plots the diffusivity and reaction-rate functions, $D(r)$ and $k(r)$, obtained using the above procedure for four different choices of α and set parameter values for $[D_{\min}, D_{\max}]$ and $[k_{\min}, k_{\max}]$ (Figure 3) [15]. Note that the smallest and largest values of α accurately approximate the two limiting cases of a homogeneous system with constant $D(r)$ and $k(r)$ ($\alpha = 0.0001$) and a composite system with stepwise $D(r)$ and $k(r)$ ($\alpha = 10000$).

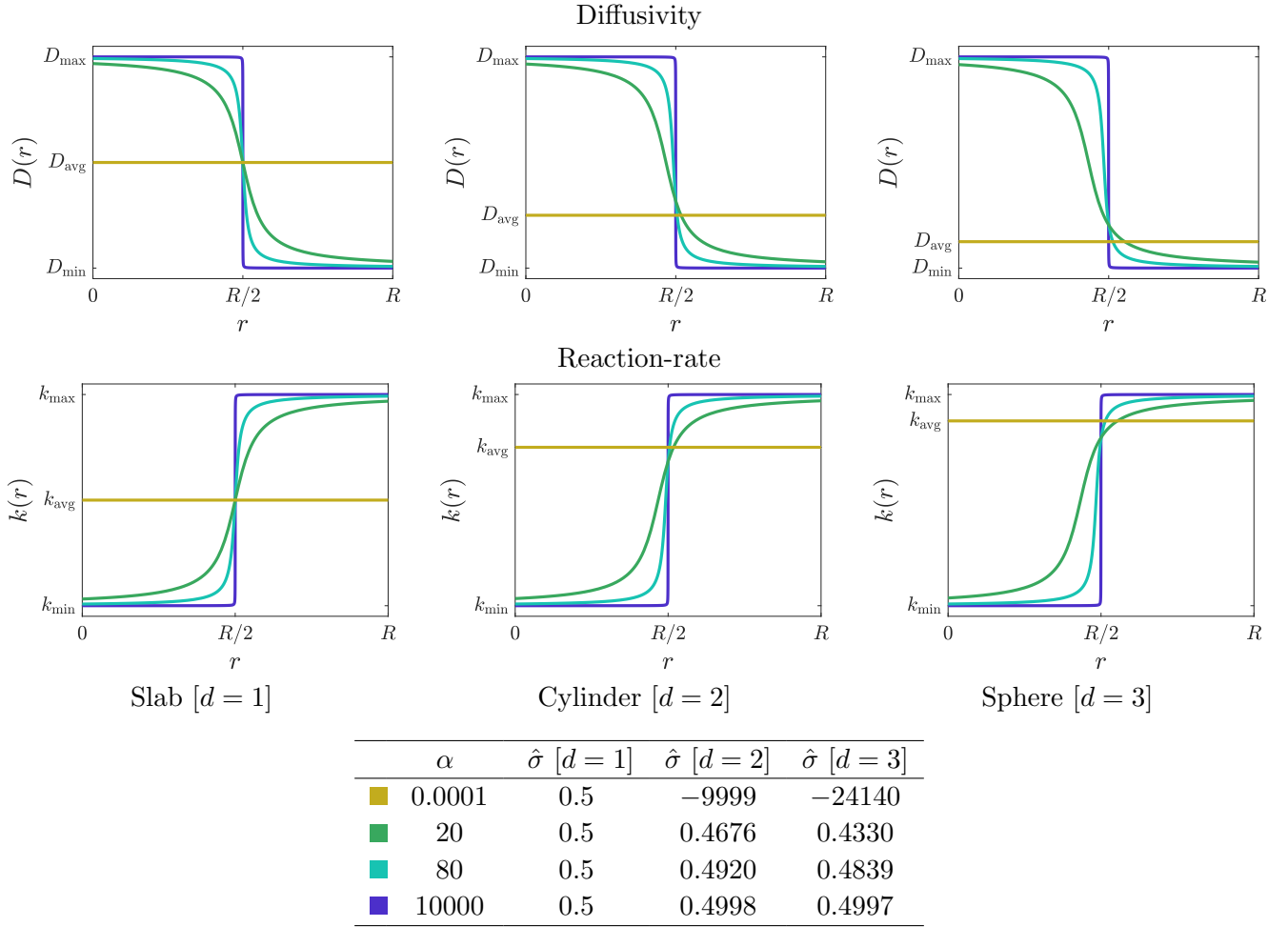


Figure 3: Functionally-graded diffusivity and reaction-rate functions. Diffusivity $D(r)$ (top row) and reaction-rate $k(r)$ (bottom row) profiles for each device-geometry (slab, cylinder, sphere). For each value of α and d , the table provides the dimensionless value of σ satisfying equation (44), defined by $\hat{\sigma} = \sigma/R$, rounded to four significant digits. Parameters: $[D_{\min}, D_{\max}] = [10^{-13}, 10^{-11}] \text{ cm}^2 \text{ s}^{-1}$ and $[k_{\min}, k_{\max}] = [8 \cdot 10^{-5}, 10^{-4}] \text{ s}^{-1}$.

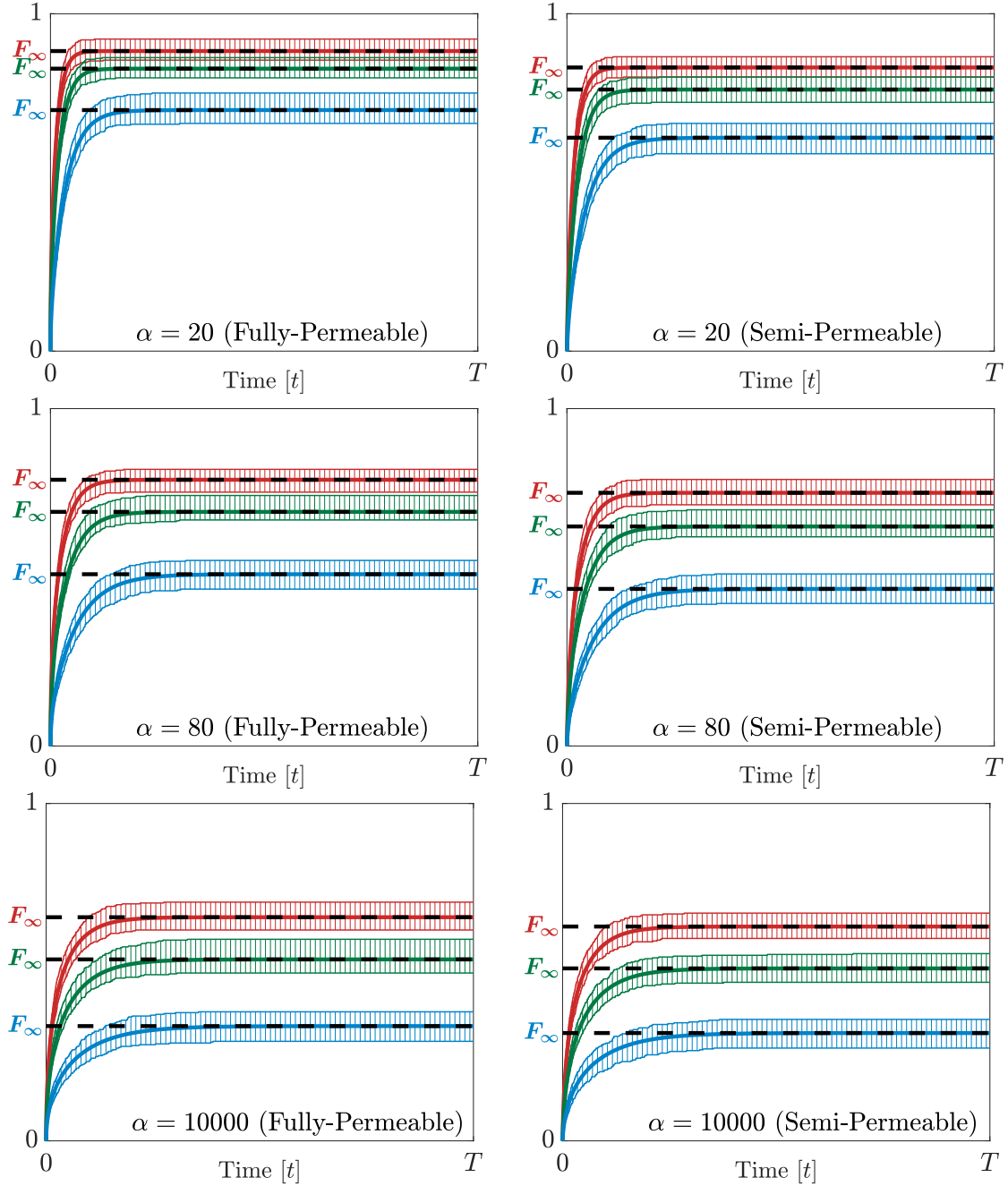
4.2 Verification of deterministic-continuum and stochastic-discrete approaches

We now verify our deterministic-continuum (section 2) and stochastic-discrete (section 3) approaches for calculating the fraction of drug released. In total, we consider 24 different test cases, one for each combination of device geometry (slab, cylinder, sphere), coating permeability (fully-permeable, semi-permeable) and α value ($\alpha = 0.0001, 20, 80, 10000$; see Figure 3). For each test case, we compare the value of F_{∞} (total fraction of drug released) obtained from the deterministic-continuum approach via the analytical formulas (30)–(35) to profiles of $F(t)$ (fraction of drug released over time) obtained from the stochastic-discrete approach via repeated simulations of the random walk algorithm (Algorithm 1). Both approaches are also benchmarked against numerical approximations of F_{∞} and $F(t)$, calculated by combining a numerical solution of the reaction-diffusion model (1)–(4) with the following analytical expressions for F_{∞} and $F(t)$ (see Appendix D for further details):

$$F_{\infty} = \lim_{t \rightarrow \infty} F(t), \quad F(t) = \frac{R^{d-1} \int_0^t -D(R) \frac{\partial c}{\partial r}(R, s) ds}{\int_0^R r^{d-1} c_0(r) dr}. \quad (47)$$

Results presented in Figure 4 show good agreement between all methods for calculating the fraction of drug released. In particular, for each of the 24 test cases: the deterministic-continuum (analytical) value of F_{∞} falls within the limiting behaviour of the stochastic-discrete profile of $F(t)$; the deterministic-continuum (analytical) value of F_{∞} agrees with the numerical estimate of F_{∞} to four significant figures; and the stochastic-discrete profile of $F(t)$ envelopes the numerical profile of $F(t)$. In summary, these results provide strong evidence to support the accuracy of both the deterministic-continuum and stochastic-discrete approaches developed in this paper.

In addition to verifying our mathematical working, several physical observations can also be drawn from



		Fully-Permeable			Semi-Permeable		
α	Method	$d = 1$	$d = 2$	$d = 3$	$d = 1$	$d = 2$	$d = 3$
0.0001	Analytical	0.9445	0.9566	0.9546	0.8073	0.8769	0.8988
	Numerical	0.9445	0.9566	0.9546	0.8073	0.8769	0.8988
20	Analytical	0.7145	0.8372	0.8894	0.6325	0.7753	0.8407
	Numerical	0.7145	0.8372	0.8894	0.6325	0.7753	0.8407
80	Analytical	0.5091	0.6940	0.7891	0.4656	0.6507	0.7505
	Numerical	0.5091	0.6940	0.7891	0.4656	0.6507	0.7505
10000	Analytical	0.3402	0.5378	0.6629	0.3196	0.5112	0.6352
	Numerical	0.3402	0.5378	0.6629	0.3196	0.5112	0.6352

Figure 4: Verification of deterministic-continuum and stochastic-discrete approaches. Plots depict the analytical values of F_∞ computed using equations (30)–(35) (dashed line) and stochastic-discrete profiles of $F(t)$ computed using Algorithm 1 (enveloping regions), benchmarked against numerical approximations to $F(t)$ as per Appendix D (solid line). For the stochastic-discrete approach, the enveloping regions extend between the 10% and 90% quantiles across 100 trials of Algorithm 1. Table compares the analytical values of F_∞ computed using equations (30)–(35) to benchmark numerical values of F_∞ computed as per Appendix D. Results are given for each combination of device geometry (\blacksquare $d = 1$ (slab); \blacksquare $d = 2$ (cylinder); \blacksquare $d = 3$ (sphere)), coating permeability (fully-permeable, semi-permeable), and α value (prescribing $D(r)$ and $k(r)$ as in Figure 3). Note colour coding for $d = 1, 2, 3$ applies across all plots and the table. The profiles for $\alpha = 0.0001$ show equivalent levels of agreement but are not shown since the stochastic-discrete enveloping regions greatly overlap when visualised. Parameters: $N_s = 400$ (analytical); $M = 51$, $N_t = 1.5 \cdot 10^6$, $N_p = 200$ (stochastic); $M = 5001$, $N_t = 10^4$ (numerical); $c_0(r) = 0.4 \text{ mol cm}^{-3}$, $R = 10^{-4} \text{ cm}$, $P = 5 \cdot 10^{-8} \text{ cm s}^{-1}$, $T = 10^5 \text{ s}$.

the results presented in Figure 4. First, we see that F_∞ increases when d increases, which is explained by the fact that drug particles are more likely to move outwards towards the release surface ($r = R$) than inwards for cylinder and sphere geometries ($d = 2, 3$) and the fact that this biased movement towards the release surface is more pronounced when d increases [34]. Second, we see that F_∞ is larger for fully-permeable coatings than for semi-permeable coatings. This is easily explained by the fact that semi-permeable coatings reject the release of some drug particles at the release surface ($r = R$) prolonging their time within the device and therefore increasing the likelihood that they undergo a binding event and never be released. Finally, we see that F_∞ decreases when α increases. This is explained by the fact that drug particles are both more likely to undergo a binding event and less likely to undergo a movement event in $(R/2, R)$ (further increasing the likelihood they undergo a binding event at some stage) when α is large, which results in less drug particles being released.

4.3 Reproduction of previous results

In previous work, Carr [22] developed analytical expressions for F_∞ for two special cases of the reaction-diffusion model (1)–(4) corresponding to a monolithic and core-shell system, respectively. The monolithic system considers constant values for the diffusivity $D(r)$, reaction-rate $k(r)$ and initial concentration $c_0(r)$, whereas the core-shell system considers step-wise functions (with no binding in the core):

Monolithic system:

$$D(r) = D, \quad k(r) = k, \quad c_0(r) = c_0, \quad 0 < r < R, \quad (48)$$

Core-shell system:

$$D(r) = \begin{cases} D_c, & 0 < r < R_c, \\ D_s, & R_c < r < R, \end{cases} \quad k(r) = \begin{cases} 0, & 0 < r < R_c, \\ k_s, & R_c < r < R, \end{cases} \quad c_0(r) = \begin{cases} c_0, & 0 < r < R_c, \\ 0, & R_c < r < R. \end{cases} \quad (49)$$

We now show how our formulas for F_∞ can be applied to replicate both the monolithic and core-shell cases. For the monolithic case, we simply choose $D(r)$, $k(r)$ and $c_0(r)$ to be constant as in equation (48). For the core-shell case, however, we cannot work with discontinuous step-wise $D(r)$, so we use smooth approximations to $D(r)$ and $k(r)$ as in (40)–(41) with $D_{\max} = D_c$, $D_{\min} = D_s$, $k_{\min} = 0$ and $k_{\max} = k_s$.

Tables 1 and 2 compare values of F_∞ obtained using the analytical expressions developed in the current paper (equations (30)–(35)) to those obtained using the analytical expressions of Carr [22] for both the monolithic and core-shell systems. For the monolithic system, we see that the reported values of F_∞ agree to the four decimal places reported for each combination of device geometry ($d = 1, 2, 3$ for slab, cylinder, sphere) and coating permeability (fully-permeable, semi-permeable). For the core-shell system, the values of F_∞ computed using our formulas approach those of Carr [22] as α increases (i.e. as $D(r)$ and $k(r)$ become closer to step-wise functions). In summary, these results provide further evidence to support the analytical expressions for F_∞ developed.

Formula Set	Fully-Permeable			Semi-Permeable		
	$d = 1$	$d = 2$	$d = 3$	$d = 1$	$d = 2$	$d = 3$
Current paper	0.8611	0.9423	0.9682	0.7928	0.8999	0.9379
Carr (2024)	0.8611	0.9423	0.9682	0.7928	0.8999	0.9379

Table 1: Comparison to Carr’s (2024) monolithic formulas. Calculated values of F_∞ obtained using the analytical expressions developed in the current paper (equations (30)–(35)) to those obtained using the monolithic analytical expressions developed previously by Carr (2024) (equations (10)–(15) in [22]). Results are given for each combination of device geometry ($d = 1, 2, 3$ for slab, cylinder, sphere) and coating permeability (fully-permeable, semi-permeable). Parameter values: $D(r) = 10^{-12} \text{ cm}^2 \text{ s}^{-1}$, $k(r) = 5 \cdot 10^{-5} \text{ s}^{-1}$, $c_0(r) = 0.4 \text{ mol cm}^{-3}$, $R = 10^{-4} \text{ cm}$, $P = 5 \cdot 10^{-8} \text{ cm s}^{-1}$, $N_s = 400$ [Current paper]; $D = 10^{-12} \text{ cm}^2 \text{ s}^{-1}$, $k = 5 \cdot 10^{-5} \text{ s}^{-1}$, $R = 10^{-4} \text{ cm}$, $P = 5 \cdot 10^{-8} \text{ cm s}^{-1}$ [Carr (2024)].

Formula Set	α	Fully-Permeable			Semi-Permeable		
		$d = 1$	$d = 2$	$d = 3$	$d = 1$	$d = 2$	$d = 3$
Current paper	10^2	0.5959	0.6466	0.6885	0.5566	0.6115	0.6573
	10^3	0.4283	0.4841	0.5345	0.4041	0.4609	0.5125
	10^4	0.3986	0.4533	0.5033	0.3767	0.4319	0.4830
	10^5	0.3952	0.4496	0.4995	0.3735	0.4285	0.4794
Carr (2024)	NA	0.3948	0.4493	0.4994	0.3731	0.4283	0.4792

Table 2: Comparison to Carr’s (2024) core-shell formulas. Calculated values of F_∞ obtained using the analytical expressions developed in the current paper (equations (30)–(35)) to those obtained using the core-shell analytical expressions developed previously by Carr (2024) (equations (29)–(34) in [22]). Results are given for each combination of device geometry ($d = 1, 2, 3$ for slab, cylinder, sphere) and coating permeability (fully-permeable, semi-permeable). Parameter values: $D(r)$ and $k(r)$ as per Figure 3 except with $k_{\min} = 0 \text{ s}^{-1}$, $c_0(r) = 0.4[1 - H(r - R/2)] \text{ mol cm}^{-3}$, $R = 10^{-4} \text{ cm}$, $P = 5 \cdot 10^{-8} \text{ cm s}^{-1}$, $N_s = 400$ [Current paper]; $D_c = 10^{-11} \text{ cm}^2 \text{ s}^{-1}$, $D_s = 10^{-13} \text{ cm}^2 \text{ s}^{-1}$, $k_s = 5 \cdot 10^{-5} \text{ s}^{-1}$, $c_0 = 0.4 \text{ mol cm}^{-3}$, $R = 10^{-4} \text{ cm}$, $R_c = 0.5 \cdot 10^{-4} \text{ cm}$, $P = 5 \cdot 10^{-8} \text{ cm s}^{-1}$ [Carr (2024)].

5 Conclusions

Recent research has highlighted the advantages of functionally-graded materials (FGMs) in drug delivery systems to achieve desired release profiles, and revealed how it is possible for drug particles to undergo a binding reaction and become irreversibly immobilised within the system. In this paper, we have presented novel deterministic-continuum and stochastic-discrete approaches for extracting insight into the drug release profile, $F(t)$, for functionally-graded delivery systems with binding reactions.

The foundation of both approaches is a recently established reaction-diffusion model of drug release in the presence of binding reactions, where a first-order reaction term captures the binding reactions, and smooth spatially-varying diffusivity and reaction rate functions reflect the functionally-graded material [15]. The deterministic-continuum approach, outlined in Section 2, yielded exact analytical expressions for calculating the total fraction of drug released, $F_\infty := \lim_{t \rightarrow \infty} F(t)$. This was achieved by expressing F_∞ in terms of the solution of a boundary value problem (derived from the governing reaction-diffusion model) and then solving analytically using a generalised eigenfunction expansion technique. The stochastic-discrete approach, outlined in Section 3, developed a random walk model of the drug release process capturing variability in $F(t)$ and F_∞ . This was achieved by discretising the governing reaction-diffusion model in space and time to derive probabilities governing the movement, binding and release of individual drug particles. Simulation results presented in Section 4 showed that both approaches are in good agreement with benchmark numerical approximations of F_∞ and/or $F(t)$, and that the deterministic-continuum approach is able to reproduce values of F_∞ obtained from the formulas derived in [22] for the two limiting cases of the monolithic and core-shell system.

In summary, we have provided new analytical and computational tools for exploring the effect of system parameters (diffusivity and reaction rate functions, geometry of the device, coating permeability) on the drug release, insight which may be useful for designers and manufacturers of drug delivery systems. While both the deterministic-continuum and stochastic-discrete approaches are valid for general smooth diffusivity and reaction-rate functions, $D(r)$ and $k(r)$, it is important to note that they are both limited to the specific device configurations illustrated in Figure 2, namely, radially-symmetric slab, cylinder and sphere geometries uniformly encapsulated in a thin coating that is either fully-permeable (zero resistance to drug release) or semi-permeable (finite resistance to drug release). Extending the deterministic-continuum and/or stochastic-discrete approaches to relax some of these assumptions, e.g. angular-dependent diffusivity and reaction-rate or non-uniform boundary conditions at the release surface, could be interesting and challenging directions for future research.

CRedit authorship contribution statement

Obi A. Carwood: Writing – original draft, Writing – review & editing, Formal analysis, Methodology, Validation, Visualization, Investigation, Software, Data Curation, Funding acquisition. **Elliot J. Carr:** Conceptualization, Writing – review & editing, Methodology, Supervision, Funding acquisition.

Data availability

MATLAB code implementing all methods and reproducing the results of the paper is available on GitHub: <https://github.com/Obi-Carwood/Carwood2025>.

Acknowledgements

The first author completed this research as part of a Master of Philosophy (MPhil) project and acknowledges support provided by an Australian Government Research Training Program Scholarship.

Appendix A Derivation for F_∞

In this appendix, we derive the formula for F_∞ given in equation (5) for the radially-symmetric reaction-diffusion model (1)–(4). The working closely follows the working featured in [22] for the simplified monolithic system (constant values of diffusivity, reaction-rate and initial concentration). By definition, F_∞ is equal to the total cumulative amount of drug released from the device scaled by the initial amount of drug loaded into the device. Mathematically, this can be represented in terms of the concentration flux [22]:

$$F_\infty = \frac{\int_0^\infty \iint_\omega [-D \nabla c \cdot \mathbf{n} \, dA] \, dt}{\iiint_\Omega c_0 \, dV}, \quad (50)$$

where ω denotes the release surface(s) (see Figure 2), Ω is the domain occupied by the device and \mathbf{n} is the unit vector normal to ω directed outwards from Ω . Under radial-symmetry, where c , D and c_0 vary spatially in r only, we have

$$F_\infty = \frac{|\omega| \int_0^\infty -D(R) \frac{\partial c}{\partial r}(R, t) \, dt}{|\Psi| \int_0^R r^{d-1} c_0(r) \, dr}, \quad (51)$$

where $|\omega|$ is the area of ω and $|\Psi|$ is the constant obtained by integrating out the non-radial coordinates in the denominator of (50), with both quantities depending on the domain geometry ($d = 1, 2, 3$ for the slab, cylinder, sphere):

$$|\omega| = \begin{cases} LW, & \text{for } d = 1, \\ 2\pi RH, & \text{for } d = 2, \\ 4\pi R^2, & \text{for } d = 3. \end{cases} \quad |\Psi| = \begin{cases} LW, & \text{for } d = 1, \\ 2\pi H, & \text{for } d = 2, \\ 4\pi, & \text{for } d = 3. \end{cases}$$

Combining (51) with the observation that $|\omega|/|\Psi| = R^{d-1}$ for all $d = 1, 2, 3$ then yields the desired result (5):

$$F_\infty = \frac{R^{d-1} \int_0^\infty -D(R) \frac{\partial c}{\partial r}(R, t) \, dt}{\int_0^R r^{d-1} c_0(r) \, dr}.$$

Appendix B New expression for F_∞

In this appendix, we derive the new formula (7) which expresses F_∞ in terms of the solution, $C(r)$, of the boundary value problem (8)–(10). The working closely follows the working featured in [22] for the simplified monolithic system (constant values of diffusivity, reaction-rate and initial concentration). We begin by first multiplying the reaction-diffusion equation (1) by r^{d-1} and integrating over $r \in [0, R]$ to give:

$$\int_0^R r^{d-1} \frac{\partial c}{\partial t} \, dr = \int_0^R \frac{\partial}{\partial r} \left(D(r) r^{d-1} \frac{\partial c}{\partial r} \right) \, dr - \int_0^R r^{d-1} k(r) c(r, t) \, dr.$$

Next, reversing the order of the derivative and integral on the left-hand side and inserting the boundary conditions (3) on the right-hand side, we get,

$$\frac{d}{dt} \int_0^R r^{d-1} c(r, t) \, dr = D(R) R^{d-1} \frac{\partial c}{\partial r}(R, t) - \int_0^R r^{d-1} k(r) c(r, t) \, dr.$$

Integrating this equation over $t \in [0, \infty)$ then gives:

$$\int_0^R r^{d-1} \left[\lim_{t \rightarrow \infty} c(r, t) - c(r, 0) \right] dr = \int_0^\infty D(R) R^{d-1} \frac{\partial c}{\partial r}(R, t) dt - \int_0^R r^{d-1} k(r) \left(\int_0^\infty c(r, t) dt \right) dr.$$

Noting the transformation $C(r)$ (6), the initial condition (2), and the fact that $c(r, t)$ approaches zero as t tends to infinity, we get:

$$\int_0^R -r^{d-1} c_0(r) dr = \int_0^\infty D(R) R^{d-1} \frac{\partial c}{\partial r}(R, t) dt - \int_0^R r^{d-1} k(r) C(r) dr.$$

Finally, rearranging and dividing by $\int_0^R r^{d-1} c_0(r) dr$ yields:

$$\frac{R^{d-1} \int_0^\infty -D(R) \frac{\partial c}{\partial r}(R, t) dt}{\int_0^R r^{d-1} c_0(r) dr} = 1 - \frac{\int_0^R r^{d-1} k(r) C(r) dr}{\int_0^R r^{d-1} c_0(r) dr}.$$

Recall that the left-hand-side is precisely the formula for the total fraction of drug released (F_∞) given in equation (5) and hence we have derived the desired result (7):

$$F_\infty = 1 - \frac{\int_0^R r^{d-1} k(r) C(r) dr}{\int_0^R r^{d-1} c_0(r) dr}.$$

We now turn our attention to deriving the boundary-value-problem (8)–(10) satisfied by $C(r)$. Here, we begin by integrating the governing reaction-diffusion equation (1) over $t \in [0, \infty)$:

$$\int_0^\infty \frac{\partial c}{\partial t} dt = \int_0^\infty \frac{1}{r^{d-1}} \frac{\partial}{\partial r} \left(D(r) r^{d-1} \frac{\partial c}{\partial r} \right) dt - \int_0^\infty k(r) c(r, t) dt,$$

and then simplifying to yield:

$$\lim_{t \rightarrow \infty} c(r, t) - c(r, 0) = \frac{1}{r^{d-1}} \frac{d}{dr} \left(D(r) r^{d-1} \frac{d}{dr} \int_0^\infty c(r, t) dt \right) - k(r) \int_0^\infty c(r, t) dt.$$

Again, noting the transformation $C(r)$ (6), the initial condition (2), and the fact that $c(r, t)$ approaches zero as t tends to infinity, we get the differential equation satisfied by $C(r)$ as stated in equation (8), namely:

$$-c_0(r) = \frac{1}{r^{d-1}} \frac{d}{dr} \left(D(r) r^{d-1} \frac{dC}{dr} \right) - k(r) C(r).$$

Lastly, taking a similar approach of integrating the governing boundary conditions (3)–(4) over $t \in [0, \infty)$ yields the boundary conditions (9)–(10) satisfied by $C(r)$ (see [22] for further detail).

Appendix C Finite volume method

In this appendix, we discretise the reaction-diffusion model (1)–(4) in space to derive the system of ODEs given in equation (36) for the semi-permeable coating problem. Spatial discretisation is carried out using a standard vertex-centred finite volume method on a uniform spatial grid consisting of M nodes, located at $r_i = (i-1)h$ for $i = 1, \dots, M$ where $h = R/(M-1)$, and M control volumes spanning the intervals $r \in [w_i, e_i]$ for $i = 1, \dots, M$, where $w_i = \max\{0, (i-3/2)h\}$ and $e_i = \min\{(i-1/2)h, R\}$ are the “west” and “east” boundaries of control volume i , respectively. Multiplying (1) by r^{d-1} and then integrating over $[w_i, e_i]$ yields:

$$\frac{d\bar{c}_i}{dt} = \frac{D(e_i) e_i^{d-1}}{V_i} \frac{\partial c}{\partial r}(e_i, t) - \frac{D(w_i) w_i^{d-1}}{V_i} \frac{\partial c}{\partial r}(w_i, t) - \bar{k} \bar{c}_i,$$

where \bar{c}_i and $\bar{k} \bar{c}_i$ are, respectively, the averaged values of $c(r, t)$ and $k(r) c(r, t)$ over control volume i :

$$\bar{c}_i = \frac{1}{V_i} \int_{w_i}^{e_i} r^{d-1} c(r, t) dr, \quad \bar{k} \bar{c}_i = \frac{1}{V_i} \int_{w_i}^{e_i} r^{d-1} k(r) c(r, t) dr, \quad V_i = \int_{w_i}^{e_i} r^{d-1} dr,$$

with c_i denoting the approximation to $c(r_i, t)$. Using the standard finite volume approach of approximating averaged values over control volumes by the values at the corresponding nodes then gives:

$$\frac{dc_i}{dt} = \frac{D(e_i)e_i^{d-1}}{V_i} \frac{\partial c}{\partial r}(e_i, t) - \frac{D(w_i)w_i^{d-1}}{V_i} \frac{\partial c}{\partial r}(w_i, t) - k(r_i)c_i.$$

Finally, inserting the boundary conditions (3) and (4) (semi-permeable case only), which apply at $r = w_1 = 0$ and $r = e_N = R$, respectively, and using second-order central difference approximations for the remaining derivatives yields the following spatially-discrete system of ODEs:

$$\begin{aligned} \frac{dc_1}{dt} &= -\frac{D(e_1)e_1^{d-1}}{V_1h}c_1 + \frac{D(e_1)e_1^{d-1}}{V_1h}c_2 - k(r_1)c_1, \\ \frac{dc_i}{dt} &= \frac{D(w_i)w_i^{d-1}}{V_ih}c_{i-1} - \left[\frac{D(w_i)w_i^{d-1}}{V_ih} + \frac{D(e_i)e_i^{d-1}}{V_ih} \right] c_i + \frac{D(e_i)e_i^{d-1}}{V_ih}c_{i+1} - k(r_i)c_i, \quad \text{for } i = 2, \dots, M-1, \\ \frac{dc_M}{dt} &= \frac{D(w_M)w_M^{d-1}}{V_Mh}c_{M-1} - \frac{D(w_M)w_M^{d-1}}{V_Mh}c_M - k(r_M)c_M - \frac{PR^{d-1}}{V_M}c_M. \end{aligned}$$

The above system can then be expressed in the form of the ODE system (36), where coefficients of c_1, \dots, c_M involving the diffusivity $D(r)$, reaction-rate $k(r)$ and mass transfer coefficient P appear in \mathbf{A}_m , \mathbf{A}_b and \mathbf{A}_r , respectively. In summary, the non-zero entries \mathbf{A}_m , \mathbf{A}_b and \mathbf{A}_r are given by:

$$\begin{aligned} a_{1,1}^m &= -\frac{D(e_1)e_1^{d-1}}{V_1h}, \quad a_{1,2}^m = \frac{D(e_1)e_1^{d-1}}{V_1h}, \\ a_{i,i-1}^m &= \frac{D(w_i)w_i^{d-1}}{V_ih}, \quad a_{i,i}^m = -\left[\frac{D(w_i)w_i^{d-1}}{V_ih} + \frac{D(e_i)e_i^{d-1}}{V_ih} \right], \quad a_{i,i+1}^m = \frac{D(e_i)e_i^{d-1}}{V_ih}, \quad \text{for } i = 2, \dots, M-1, \\ a_{M,M-1}^m &= \frac{D(w_M)w_M^{d-1}}{V_Mh}, \quad a_{M,M}^m = -\frac{D(w_M)w_M^{d-1}}{V_Mh}, \\ a_{i,i}^b &= k(r_i), \quad \text{for } i = 1, \dots, M, \quad a_{M,M}^r = \frac{PR^{d-1}}{V_M}, \end{aligned}$$

where $a_{i,j}^m$, $a_{i,j}^b$ and $a_{i,j}^r$ denote the entries in row i and column j of \mathbf{A}_m , \mathbf{A}_b and \mathbf{A}_r , respectively.

Appendix D Numerical computation of F_∞ and $F(t)$

In section 4.2, numerical benchmark approximations are used to validate our deterministic-continuum and stochastic-discrete approaches for calculating F_∞ and $F(t)$. In this appendix, we explain how these benchmark approximations are computed by combining a numerical solution of the governing reaction-diffusion model (1)–(4) with the following analytical expression for $F(t)$:

$$F(t) = \frac{R^{d-1} \int_0^t -D(R) \frac{\partial c}{\partial r}(R, s) ds}{\int_0^R r^{d-1} c_0(r) dr}. \quad (52)$$

We solve the reaction-diffusion model (1)–(4) numerically by discretising in space using the vertex-centered finite volume method outlined in Appendix C and in time using the backward Euler method. As for the stochastic-discrete approach (Section 3), discretisation is carried out using uniform grids in both space and time, defined by $r_i = (i-1)h$ for $i = 1, \dots, M$ and $t_n = n\tau$ for $n = 1, \dots, N_t$, where $h = R/(M-1)$ and $\tau = T/N_t$ (however, we assume M and N_t may take on different values to those featuring in the stochastic-discrete approach). For each time $t = t_n$, we then compute the fraction of drug released, $F(t_n)$, by processing the following steps: (i) evaluate $F(t)$ (52) at $t = t_n$ (ii) approximate the spatial derivative, $\frac{\partial c}{\partial r}(R, s)$, using a backward-difference approximation (iii) numerically compute both the numerator and denominator integrals featuring in $F(t)$ (52) using in-built MATLAB functions. Finally, we take F_∞ to be $F(T)$ (i.e. $F(t_{N_t})$), making sure to choose T large enough to capture the limiting behaviour of $F(t)$. For full details on the computation of the numerical benchmarks, the interested reader is referred to our MATLAB code available on GitHub; see [Data availability](#).

References

- [1] N. Sahai, M. Gogoi, and N. Ahmad. Mathematical modeling and simulations for developing nanoparticle-based cancer drug delivery systems: A review. *Current Pathobiology Reports*, 9(1):1–8, 2021.
- [2] J. Siepmann and F. Siepmann. Mathematical modeling of drug delivery. *International Journal of Pharmaceutics*, 364(2):328–343, 2008.
- [3] S. Lotter, T. Bellmann, S. Marx, M. Wesinger, L. Brand, M. Schäfer, D. Fischer, and R. Schober. Microparticle-based controlled drug delivery systems: From experiments to statistical analysis and design. *GLOBECOM 2023 - 2023 IEEE Global Communications Conference*, pages 1167–1172, 2023.
- [4] R. Hernandez-Montelongo, J. Salazar-Araya, J. Hernandez-Montelongo, and J. P. Garcia-Sandoval. Mathematical modeling of recursive drug delivery with diffusion, equilibrium, and convection coupling. *Mathematics*, 10(13):2171, 2022.
- [5] J. Siepmann and F. Siepmann. Modeling of diffusion controlled drug delivery. *Journal of Controlled Release*, 161(2):351–362, 2012.
- [6] E. J. Carr and G. Pontrelli. Modelling mass diffusion for a multi-layer sphere immersed in a semi-infinite medium: application to drug delivery. *Mathematical Biosciences*, 303:1–9, 2018.
- [7] B. Kaoui, M. Lauricella, and G. Pontrelli. Mechanistic modelling of drug release from multi-layer capsules. *Computers in Biology and Medicine*, 93:149–157, 2018.
- [8] D. Y. Arifin, L. Y. Lee, and C. Wang. Mathematical modeling and simulation of drug release from microspheres: Implications to drug delivery systems. *Advanced Drug Delivery Reviews*, 58(12-13):1274–1325, 2006.
- [9] M. Gonçalves, E. Gudiño, M. Maia, and C. Oishi. Mathematical modeling for drug delivery and inflammation process: An application in macular edema. *Applied Mathematical Modelling*, 121:668–689, 2023.
- [10] A. Hadjitheodorou and G. Kalosakas. Quantifying diffusion-controlled drug release from spherical devices using Monte Carlo simulations. *Materials Science and Engineering C*, 33:763–768, 2013.
- [11] M. S. Gomes-Filho, M. A. A. Barbosa, and F. A. Oliveira. A statistical mechanical model for drug release: Relations between release parameters and porosity. *Physica A: Statistical Mechanics and its Applications*, 540:123165, 2020.
- [12] L. P. Filippini, M. J. Simpson, and E. J. Carr. Simplified models of diffusion in radially-symmetric geometries. *Physica A: Statistical Mechanics and its Applications*, 626:129067, 2023.
- [13] M. Ignacio and G. W. Slater. A lattice kinetic Monte Carlo method to study drug release from swelling porous delivery systems. *Physica A: Statistical Mechanics and its Applications*, 603:127775, 2022.
- [14] E. J. Carr. Exponential and Weibull models for spherical and spherical-shell diffusion-controlled release systems with semi-absorbing boundaries. *Physica A: Statistical Mechanics and its Applications*, 605:127985, 2022.
- [15] E. J. Carr and G. Pontrelli. Modelling functionalized drug release for a spherical capsule. *International Journal of Heat and Mass Transfer*, 222:125065, 2024.
- [16] M. Ignacio and G. W. Slater. Using fitting functions to estimate the diffusion coefficient of drug molecules in diffusion-controlled release systems. *Physica A: Statistical Mechanics and its Applications*, 567:125681, 2021.
- [17] X. Hu, C. Zhang, Y. Xiong, S. Ma, C. Sun, and W. Xu. A review of recent advances in drug loading, mathematical modeling and applications of hydrogel drug delivery systems. *Journal of Materials Science*, 59(32):15077–15116, 2024.

- [18] G. Toniolo, M. Louka, G. Menounou, N. Z. Fantoni, G. Mitrikas, E. K. Efthimiadou, A. Masi, M. Bortolotti, L. Polito, A. Bolognesi, A. Kellett, C. Ferreri, and C. Chatgililoglu. [Cu(TPMA)(Phen)](ClO₄)₂: Metallodrug nanocontainer delivery and membrane lipidomics of a neuroblastoma cell line coupled with a liposome biomimetic model focusing on fatty acid reactivity. *ACS Omega*, 3(11):14538–16397, 2018.
- [19] A. Jain, S. McGinty, G. Pontrelli, and L. Zhou. Theoretical model for diffusion-reaction based drug delivery from a multilayer spherical capsule. *International Journal of Heat and Mass Transfer*, 183:122072, 2022.
- [20] G. Pontrelli, G. Toniolo, S. McGinty, D. Peri, S. Succi, and C. Chatgililoglu. Mathematical modelling of drug delivery from pH-responsive nanocontainers. *Computers in Biology and Medicine*, 131:104238, 2021.
- [21] A. Jain, G. Pontrelli, and S. McGinty. Laplace transform based modeling of drug delivery with reversible drug binding in a multilayer tissue. *Pharmaceutical Research*, 41:1093–1107, 2024.
- [22] E. J. Carr. Total fraction of drug released from diffusion-controlled delivery systems with binding reactions. *International Journal of Heat and Mass Transfer*, 229:125712, 2024.
- [23] S. Mubarak and M. A. Khanday. Mathematical modelling of drug-diffusion from multi-layered capsules/tablets and other drug delivery devices. *Computer Methods in Biomechanics and Biomedical Engineering*, 25(8):896–907, 2021.
- [24] B. Saleh, J. Jiang, R. Fathi, T. Al-hababi, Q. Xu, L. Wang, D. Song, and A. Ma. 30 years of functionally graded materials: An overview of manufacturing methods, applications and future challenges. *Composites Part B: Engineering*, 201:108376, 2020.
- [25] Yoshikazu Shinohara. Chapter 11.2.4 - Functionally Graded Materials. In Shigeyuki Somiya, editor, *Handbook of Advanced Ceramics (Second Edition)*, pages 1179–1187. Academic Press, Oxford, second edition edition, 2013.
- [26] G. Bretti, S. McGinty, and G. Pontrelli. Modelling smart drug release with functionally graded materials. *Computers in Biology and Medicine*, 164:107294, 2023.
- [27] P. R. Johnston. Diffusion in composite media: solution with simple eigenvalues and eigenfunctions. *Mathematical and Computer Modelling*, 15(10):115–123, 1991.
- [28] C. P. Naveira-Cotta, R. M. Cotta, H. R. B. Orlande, and O. Fudym. Eigenfunction expansions for transient diffusion in heterogeneous media. *International Journal of Heat and Mass Transfer*, 52(21-22):5029–5039, 2009.
- [29] C. Liu, J. E. Szecsody, J. M. Zachara, and W. P. Ball. Use of the generalized integral transform method for solving equations of solute transport in porous media. *Advances in Water Resources*, 23:483–492, 2000.
- [30] L. Meinecke, S. Engblom, A. Hellander, and P. Lotstedt. Analysis and design of jump coefficients in discrete stochastic diffusion models. *SIAM Journal on Scientific Computing*, 38(1):A55–A83, 2016.
- [31] A. Q. Cai, K. A. Landman, and B. D. Hughes. Modelling directional guidance and motility regulation in cell migration. *Bulletin Mathematical Biology*, 68:25–52, 2006.
- [32] A. R. A. Anderson and M. A. J. Chaplain. Continuous and discrete mathematical models of tumor-induced angiogenesis. *Bulletin Mathematical Biology*, 60:857–900, 1998.
- [33] E. J. Carr. Random walk models of advection-diffusion in layered media. *Applied Mathematical Modelling*, 141:115942, 2025.
- [34] E. J. Carr. Diffusion in heterogeneous discs and spheres: New closed-form expressions for exit times and homogenization formulas. *Journal of Chemical Physics*, 153:074115, 2020.